



Mechanism of Roof Cutting and Stress Relief in Coal Seams with Hard Sandstone Coverage

Peng Kong · Chang Liu · Dechuan Yang ·
Li Shihui · Jin Ruiju

Received: 20 February 2024 / Accepted: 23 May 2024 / Published online: 10 June 2024
© The Author(s), under exclusive licence to Springer Nature Switzerland AG 2024

Abstract Blasting roof cutting when the working face is directly covered with a hard roof can change the roof structure, which is an important factor for preventing dynamic disasters induced by hard roofs. This article used theoretical analysis to establish an expression for the distribution of the side abutment stress near the end of the working face before and after roof cutting. The stress reduction showed a power function growth trend with increasing crack zone height and a linear growth trend with increasing cantilever length of the hard roof. The results of the theoretical analysis provide a new approach for evaluating the effect of roof cutting and stress relief. The numerical simulation method was used to analyze the stress and plastic zone of the stope and the deformation characteristics of the roadway after roof cutting. The results showed that the advance and side abutment stresses of the working face decreased after roof cutting, and the range of the roof plastic zone increased. In addition, the displacements of the sides and floor of the roadway were reduced after roof

cutting, which is beneficial for roadway stability control. Based on the research results, the roadway support scheme was optimized, and the advance support of the roadway was removed. This greatly reduced the work intensity and support cost and ensured the stability of the roadway.

Keywords Roof cutting · Hard sandstone · Side abutment stress · Roadway · Dynamic disaster

1 Introduction

With the continuous increase in coal demand and the deterioration of mining conditions, coal seams with hard roofs account for one-third of the total coal reserves in China and are distributed in more than 50% of mining areas. Due to the characteristics of hard roofs, such as high hardness, high strength, good compactness and low joint fissure development, hard roof strata exist above coal seams during coal mining, and it is difficult for the roof to collapse naturally (Zhao et al. 2024; Kumar et al. 2022; Rajwa et al. 2019). Especially under the condition of a hard roof directly above the working face, the first weighting and periodic weighting steps and strength of the roof increase obviously. The large area of the hard roof causes the stress concentration of the surrounding rock of the roadway to increase, and its sudden collapse releases a large amount of elastic energy, which can easily lead to the collapse of the working face,

P. Kong · C. Liu (✉) · D. Yang
School of Mining Engineering, Anhui University
of Science and Technology, Huai Nan, China
e-mail: 17854859770@163.com

P. Kong
Engineering Laboratory for Safe and Precise Coal Mining
of Anhui Province, Huai Nan, China

Li. Shihui · J. Ruiju
Huaihe Energy Group, Huai Nan, China

gas outbursts, rock bursts and other safety accidents (Guo et al. 2024; Ghosh and Sivakumar 2018; Mondal et al. 2017).

Research shows that the directional cutting of roofs can reduce the stress transfer of some roofs as well as the stress concentration of the surrounding rock, and the pressure relief effect is remarkable. This approach is important for preventing dynamic disasters induced by hard roofs (Xie et al. 2018; Konicek et al. 2013). At present, the commonly used roof cutting methods are hydraulic fracturing and blasting. Compared with the hydraulic fracturing method, the blasting method is relatively simpler for roof cutting operations, the adaptability to roof conditions is stronger, and the expansion direction of blasting cracks is easier to control (Osipov 2017; Wojtecki and Gola 2020; Sainoki et al. 2017). Research shows that roof cutting can effectively reduce the roof breaking step, dynamic load coefficient and stope stress, which is highly important for the control of roadway stability (Wang et al. 2023; Zhang et al. 2024).

Roof cutting can completely cut off the connection between the roof of the goaf and the roof of the roadway by carrying out geomechanical model experiments, thus reducing the roof stress near the goaf (Wang et al. 2020; Wojtecki et al. 2020; Vennes et al. 2020; Mishra et al. 2013). Ko et al. (2022), Xu et al. (2019) studied the formation and expansion of blasting roof cracks by means of theoretical analysis and field tests and improved the blasting effect by optimizing the charging and detonation methods. Dang et al. (2024), Xu et al. (2023), Sun et al. (2024) studied the influence of roof cutting parameters on the roof breaking law and surrounding rock stress of stopes via theoretical analysis and numerical simulation, which provided a theoretical basis for quantitatively determining roof cutting parameters. The variation in the roof overburden structure after roof cutting is the key to reducing the stress of the stope and promoting the stability of the roadway. However, quantitative theoretical research results on the degree of pressure relief in stopes after roof cutting are lacking. Therefore, it is highly important to further study roof structural characteristics under the influence of roof cutting, especially the roof structure and load transfer law at the end of the working face, to reveal the mechanism of roof cutting and pressure relief under hard roof conditions.

This article is based on the engineering background of the 11,618 (east) working face in the Xieqiao Coal Mine and uses theoretical analysis methods to establish a model of the roof structure under a hard sandstone roof. The distribution pattern of the abutment stress near the end of the working face before and after roof cutting was analyzed. The law of stress reduction after roof cutting under different influencing factors was revealed, which provided a new method for evaluating the effect of roof cutting and pressure relief. The FLAC3D numerical simulation was used to analyze the stress, displacement and other multifield evolution laws of the stope and roadway after hard roof cutting. Based on the research results, the roadway support scheme was optimized, and the advance support of the roadway was removed. This greatly reduced the work intensity and support cost and ensured the stability of the roadway. The research results provide theoretical guidance for the safe mining of working faces under hard roof conditions.

2 Engineering Background

The Xieqiao Coal Mine is located in Huainan city, Anhui Province, China. The 11,618 (east) mining panel of the No. 11 coal seam has a thickness of 0–4.8 m and an average thickness of 3.1 m. The average inclination angle of the coal seam is 14°. The advancing length of the panel is 1000 m, and the inclined length is 230 m. The west side of the working face is the protective coal pillar of the system roadway, the east side is the Fzt6 fault, which is adjacent to the protective coal pillar of the mine boundary, and the south and north sides are all unexploited areas. The layout of the 11,618 panel (east) is shown in Fig. 1. The elevation of the tailgate roadway is –628.2 to 680.2 m, and the elevation of the haulage roadway is –679.3 to 729.5 m.

The fault structures in the working face are developed, of which there are two with a decrease greater than 3 m and six with a decrease less than 3 m. There is no magmatic rock mass or collapse column in the working face. The roof of the working face locally contains sandstone fissure water, which is a static reserve consumption type. During the mining period of the working face, there is a drip phenomenon in the local roof, but the amount of water is small and has little effect on the safe mining of the working

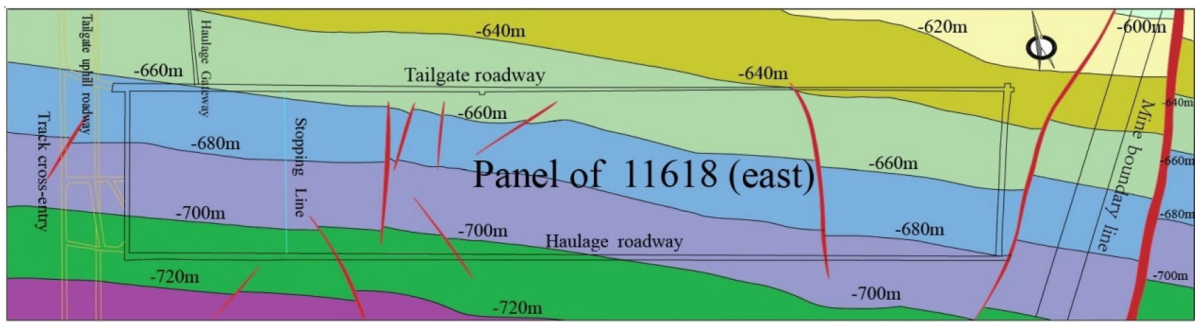


Fig. 1 Layout of Panel 11,618 (east)

face. Based on the in situ stress test results, the maximum principal stress is the vertical stress, the minimum horizontal principal stress direction is generally perpendicular to the working face advancing direction, and the lateral pressure coefficient is 0.64. The direction of the maximum horizontal principal stress is generally parallel to the advancing direction of the working face, and the lateral pressure coefficient is 0.83.

The rock stratum above the fine sandstone is quartz sandstone, and the histogram of the roof and floor rock strata of Panel 11,618 (east) is shown in Fig. 2. The fine sandstone directly covers the coal seam, with a thickness ranging from 4.4 to 16.7 m and an average thickness of 8.9 m. The fine sandstone is dense, hard, and has strong integrity. The average uniaxial compressive strength of the fine sandstone reaches 180 MPa. It has a fine-grained sandy structure and is mainly composed of quartz, followed by feldspar. The rock layer within 40 m above the fine sandstone is mainly composed of siltstone, mudstone, and sandy mudstone, with uniaxial compressive strengths not exceeding 80 MPa. Therefore, the fine sandstone controls the breaking of the roof strata and has a significant impact on the roof structure. Blasting roof cutting of hard fine sandstone can reduce the cantilever length and the risk of rockburst, and the propagation velocity of blast wave in the surrounding rock is 3000–5500 m/s.

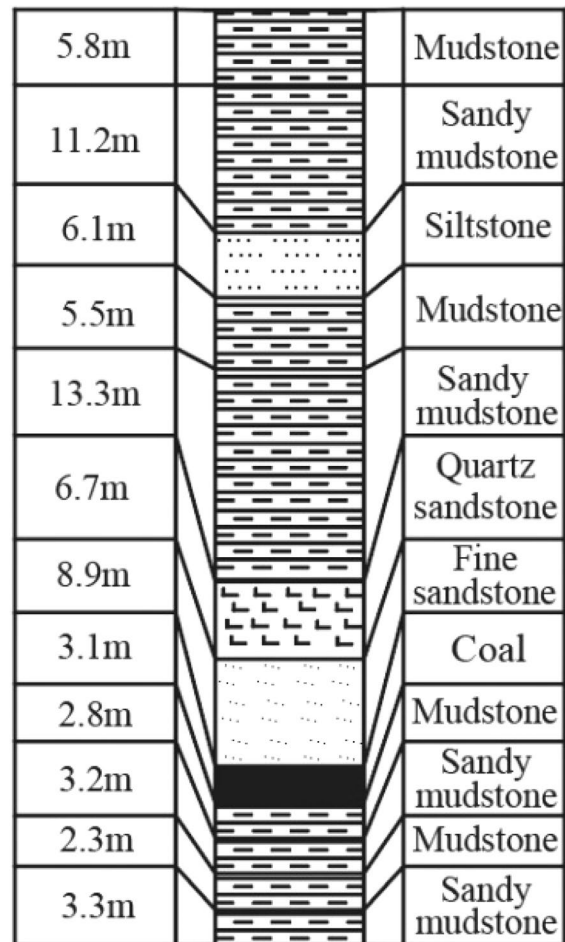


Fig. 2 Histogram of Panel 11,618 (east)

3 Methodology

3.1 Mechanical Model of the Roof Structure

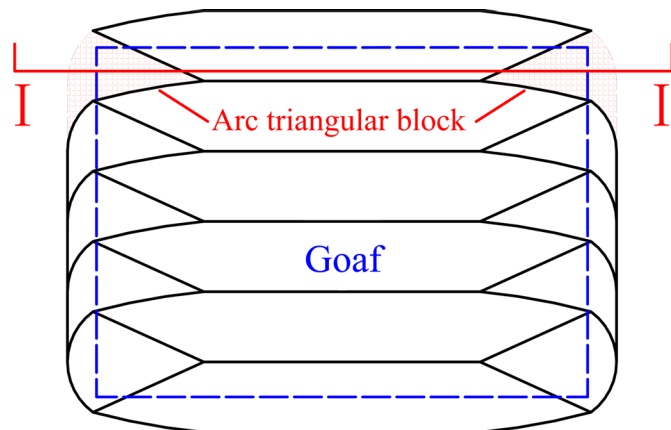
In the process of advancing the working face, the coal was continuously mined. Under the condition of the hard sandstone direct coverage on coal seam, the roof does not fall with mining but is suspended within a certain range above the goaf. With the expansion of the suspended roof, the load continuously accumulates in the roof. When the stress applied by the overlying strata exceeds the strength limit of the hard roof strata, the hard roof strata will break and sink.

Before the first collapse of the hard roof, the suspended roof can be regarded as a four-sided fixed plate, and the maximum bending moment is located at the center of the long side of the plate. Therefore, with the continuous mining of the working face, the center of the roof is the first to break. Subsequently, cracks form in the middle of the short side of the roof. After the cracks at the edge of the plate expand and penetrate, the strength of the plate itself cannot be effectively loaded and fractured; finally, an X-shaped fracture forms, and the roof breaks. After the roof first breaks, the roof above the working face loses

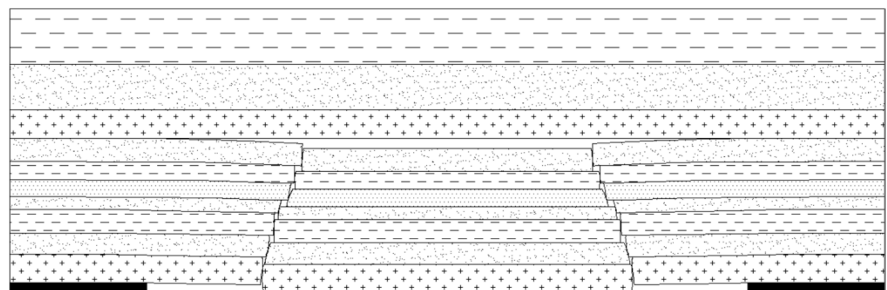
support on one side. At this time, the suspended roof can be regarded as a three-sided fixed support and a simply supported plate on one side. At this time, the maximum bending moment is located at the long side of the plate. Therefore, the long side will break after reaching its strength limit, forming a K-shaped fracture, and the roof begins to collapse periodically with the continuous advancement of the working face.

The breaking form of the end position of the working face differed from that of the middle of the working face. The roof near the end forms an arc triangular block structure, as shown in Fig. 3a. At this time, the overlying strata load at the middle position of the working face enters the goaf with the periodic break of the roof, but the roof of the triangular block on both sides of the working face is not completely broken, and it is still in the suspended roof state. The overlying strata load of the suspended roof cannot enter the goaf and transfer to the coal and rock on both sides of the working face, which leads to an increase in the side abutment stress. Therefore, the

Fig. 3 Roof structure. **a** Plane diagram of the roof structure, **b** roof structure I–I profile



(a) Plane diagram of the roof structure



(b) Roof structure I–I profile

hard fine sandstone above the coal seam was regarded as a beam structure, and the roof of the arc triangular block area was considered as a cantilever beam. The mechanical model shown in Fig. 3b was established to provide a basis for analyzing the distribution of lateral abutment stress under the condition of a hard roof.

3.2 Numerical Simulation Model and Rock Mass Parameters

Using the large-scale three-dimensional finite difference numerical simulation software FLAC3D and taking the 11,618 (east) working face of the Xieqiao Coal Mine as the engineering background, a comparative analysis was conducted on the stress evolution of the mining area and the deformation law of the roadway before and after roof cutting. The numerical calculation model is shown in Fig. 4, with a model size of length (Y) × width (X) × height (Z) of 450 m × 430 m × 160 m. To eliminate the influence of boundary effects in the numerical calculation process, the distance between the working face and the model boundary was not less than 100 m, and the simulated coal seam burial depth was 700 m. The bulk density of the nonsimulated rock layer above the model was assumed to be 25 kN/m³, and the equivalent load of the nonsimulated rock layer was calculated to be 14.5 MPa, which was applied to the upper boundary of the model.

Two sets of numerical simulation experiments were conducted, with and without roof cutting. The

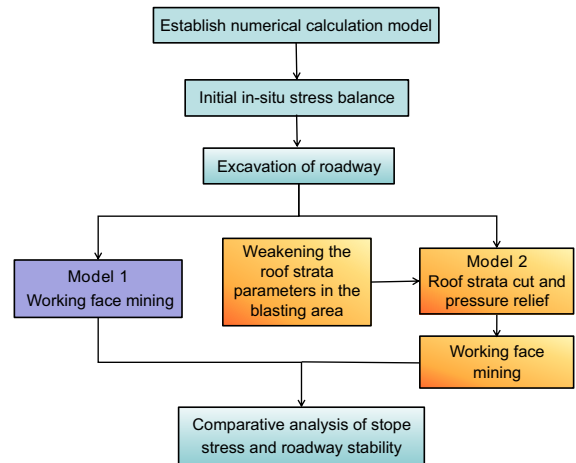
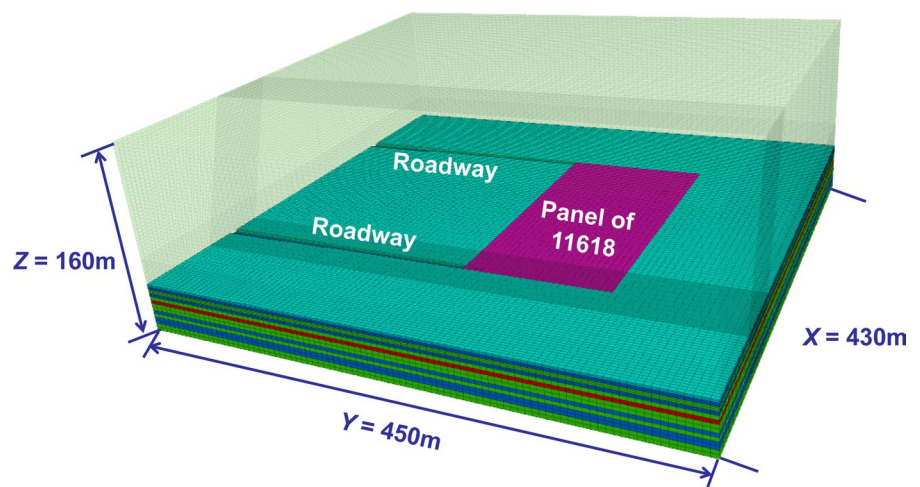


Fig. 5 Flowchart of the numerical simulation calculations

numerical calculation process is shown in Fig. 5. When conducting the numerical calculations, the initial geostress balance was first determined. Based on the geostress test results, the lateral pressure coefficient in the X direction was taken as 0.64, and the lateral pressure coefficient in the Y direction was taken as 0.82. Then, the excavation of the mining roadway proceeded. After roadway excavation, Model 1 simulates the mining of the working face, in which the working face undergoes distributed excavation with a step distance of 20 m each time. Model 2 simulates roof blasting cutting before mining the working face, decreasing the rock mass parameters in the blasting area to 1/5 of the original values, and thus simulating

Fig. 4 Numerical calculation model



cutting of the hard roof (Wang et al. 2023; Ahmet and Murat 2022).

To ensure the validity of the data, accuracy of the results, and rigor of the research, the rock strength analysis software Roclab, developed by the Hoek Brown strength criterion, was used to calculate the rock mechanics parameters involved in the numerical simulation based on the coal rock mechanics parameters obtained from laboratory experiments (Karolina and Pawelus 2021; Ganesan and Mishra 2024). The mechanical parameters of the coal and rock mass are shown in Table 1. The coal and rock mass in the numerical calculation adopted the Mohr–Coulomb strain softening model to soften the cohesion, and the ratio of residual cohesion to initial cohesion was taken as 1/5 (Zabolotnii et al. 2021; Kumar et al. 2024).

4 Results

4.1 Mechanical Model of the Roof Structure and Distribution Characteristics of the Side Abutment Stress Before Roof Cutting

Because the fine sandstone above the working face has a high strength (180 MPa) and large thickness (8.9 m), the fine sandstone was the basic roof. The roof above the fine sandstone was mainly composed of mudstone and sandstone, and the strength was less than 80 MPa. Fine sandstone controls the movement of multiple layers of rock on the roof and plays a controlling role in the roof structure.

The mechanical model of the roof structure shown in Fig. 6 was established. In the figure, α is the movement angle of the rock stratum. The side abutment stress of the working face was mainly composed of three parts. The first part is the self-weight stress σ_z of the rock mass. The second part is the load of the

Table 1 Coal and rock mass properties

Lithology	E (GPa)	ν	C (MPa)	σ (MPa)	φ ($^\circ$)	c_r (MPa)	ε_p (%)
Fine sandstone	28.9	0.22	8.6	7.3	48	0.86	0.01
Quartz sandstone	17.0	0.23	6.1	5.4	45	0.61	0.01
Mudstone	6.9	0.31	2.8	2.4	38	0.31	0.01
Sandy mudstone	8.1	0.30	3.2	2.7	40	0.30	0.01
Coal	2.4	0.34	1.8	1.3	36	0.18	0.01
Siltstone	12.7	0.25	5.4	4.8	43	0.54	0.01

E_m is the elastic modulus, μ is Poisson's ratio, C is cohesive, σ is tensile strength, φ is the internal friction angle, c_r is the residual cohesive, and ε_p is the plastic strain when the strength of the rock mass becomes residual

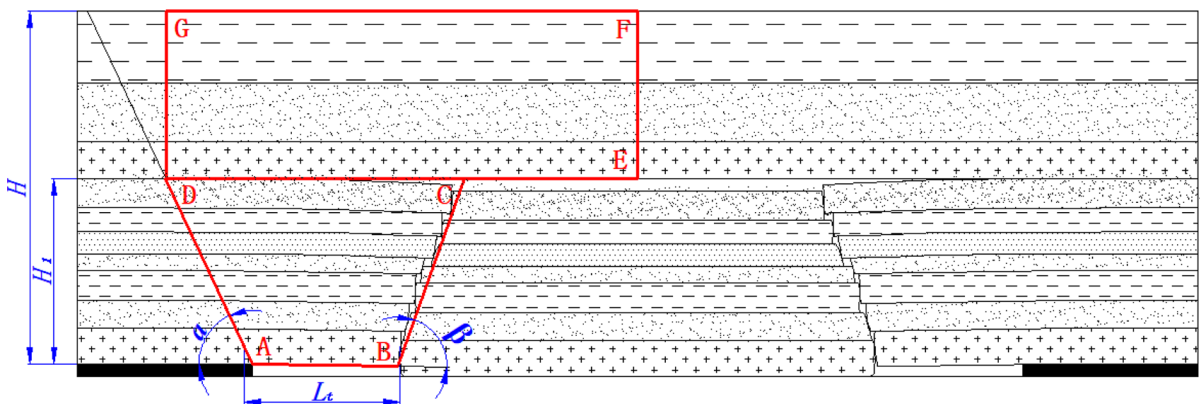


Fig. 6 Mechanical model of roof structure before roof cutting

hard sandstone cantilever beam and the broken rock block above it, as shown in the ABCD region. The third part is the load transmitted by the rock mass of the bending zone. The load of the rock mass of the bending zone was shared by the coal bodies on both sides of the goaf, as shown in the DEFG area in the figure. The load of the bending zone can be considered a uniformly distributed load, which directly acts on the rock mass of the fracture zone, and the load is transmitted to the side coal body of the goaf through the rock mass of the fracture zone. The sum of the second part load and the third part load was expressed by σ_l . Therefore, the side abutment stress σ of the working face can be expressed as Shang et al. (2022), Sun et al. (2022):

$$\sigma = \sigma_z + \sigma_l \tag{1}$$

The self-weight stress σ_z can be expressed by a set of piecewise functions:

$$\sigma_z = \begin{cases} \frac{\gamma H x \tan \alpha}{H_1}, & \left[0, \frac{H_1}{\tan \alpha}\right] \\ \gamma H, & \left(\frac{H_1}{\tan \alpha}, +\infty\right) \end{cases} \tag{2}$$

where γ is the density of the rock mass, N/m^3 ; H_1 is the fracture zone development height, m; H is the coal seam burial depth, m; and α is the stratum movement angle, $^\circ$.

After fitting the stress distribution results are measured in the field within the allowable accuracy range of the project, we can consider the distribution of the additional load as a triangular distribution. Therefore, the stress σ_l transmitted by the fracture zone and the bending zone can be expressed as:

$$\sigma_l = \begin{cases} \frac{2\sigma_{lmax} x \tan \alpha}{H_1}, & \left[0, \frac{H_1}{2 \tan \alpha}\right] \\ 2\sigma_{lmax} \left(1 - \frac{x \tan \alpha}{H_1}\right), & \left(\frac{H_1}{2 \tan \alpha}, \frac{H_1}{\tan \alpha}\right) \\ 0, & \left[\frac{H_1}{\tan \alpha}, +\infty\right] \end{cases} \tag{3}$$

The maximum value σ_{lmax} of the additional stress transmitted by the fracture zone and the bending zone can be expressed as follows:

$$\sigma_{lmax} = \frac{2\gamma \left\{ \left[L_t + \frac{H_1(\cot \alpha + \cot \beta)}{2} \right] H_1 + (115 + H_1 \cot \alpha)(H - H_1) \right\}}{H_1 \cot \alpha} \tag{4}$$

According to the mining experience of the Xieqiao Coal Mine, the burial depth of coal seam H was 700 m, the strata movement angle α was 70° , the fracture zone development height H_1 was 115 m (half of the length of the working face), and the cantilever length L_t of hard fine sandstone was 40 m. Bringing the above parameters into Formulas (2), (3) and (4), the self-weight stress σ_z and the additional stress σ_l are expressed as follows:

$$\sigma_z = \begin{cases} 0.418x, & [0, 41.86] \\ 17.5, & (41.86, +\infty) \end{cases} \tag{5}$$

$$\sigma_l = \begin{cases} 5.773x, & [0, 20.93] \\ 241.70 - 5.773x, & (20.93, 41.86) \\ 0, & [41.86, +\infty] \end{cases} \tag{6}$$

Therefore, the side abutment stress of the working face $\sigma = \sigma_z + \sigma_l$ can be expressed as:

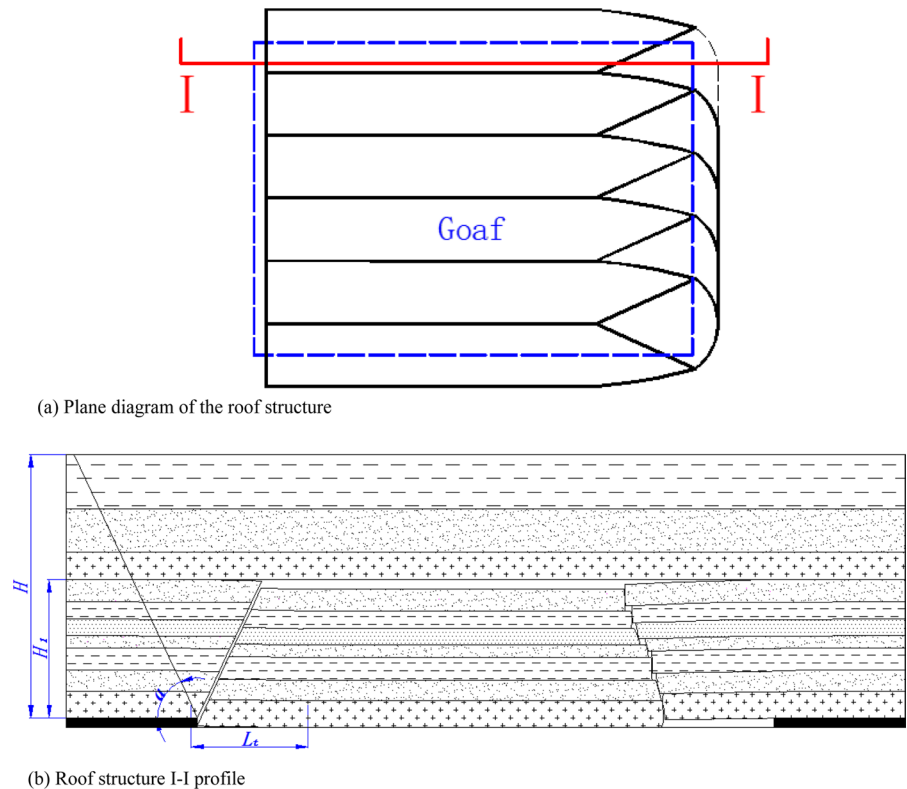
$$\sigma = \begin{cases} 6.191x, & [0, 20.93] \\ 241.70 - 5.355x, & (20.93, 41.86) \\ 17.5, & [41.86, +\infty] \end{cases} \tag{7}$$

4.2 Mechanical Model of the Roof Structure and Distribution Characteristics of the Side Abutment Stress After Roof Cutting

After the roof of the working face is cut, the cantilever beam structure of the hard roof is destroyed. The mechanical model of the roof structure after roof cutting is shown in Fig. 7. The roof on the cutting side continues to break periodically with the advancement of the working face. The arc triangular block disappears, and the load of the broken rock block above the cantilever beam is partially lifted, so it can play a role in reducing the side abutment stress. After roof cutting, the maximum value σ_{lmax} of the additional stress transmitted by the fractured zone and the bending zone can be expressed as Formula (8).

$$\sigma_{lmax} = \frac{2\gamma \left[(\cot \theta + \cot \alpha) \frac{H_1^2}{2} + (115 + H_1 \cot \alpha)(H - H_1) \right]}{H_1 \cot \alpha} \tag{8}$$

Fig. 7 Mechanical model of roof structure after roof cutting. **a** Plane diagram of the roof structure, **b** roof structure I-I profile



In the formula, θ is the cutting angle (the angle between the blasting hole and the horizontal direction), and the value is 70° .

The relevant parameters were brought into Formulas (1), (3), and (4), and the additional stress σ_l after roof cutting was obtained as follows:

$$\sigma_l = \begin{cases} 5.511x, & [0, 20.93] \\ 230.70 - 5.511x, & (20.93, 41.86) \\ 17.5, & [41.86, +\infty] \end{cases} \quad (9)$$

By substituting Formulas (3) and (9) into Formula (1), the side abutment stress σ after roof cutting can be expressed as follows:

$$\sigma = \begin{cases} 5.929x, & [0, 20.93] \\ 230.70 - 5.093x, & (20.93, 41.86) \\ 17.5, & [41.86, +\infty] \end{cases} \quad (10)$$

According to the calculation results of Formulas (7) and (10), we can obtain the distribution curve of the side abutment stress of the working face before and after roof cutting, as shown in Fig. 8. Figure 8

shows that the side abutment stress of the working face decreased after the roof was cut, and the peak of the side abutment stress decreased most sharply. The stress reduction was 5.48 MPa. Therefore, the roof cutting played a certain role in reducing the side abutment stress.

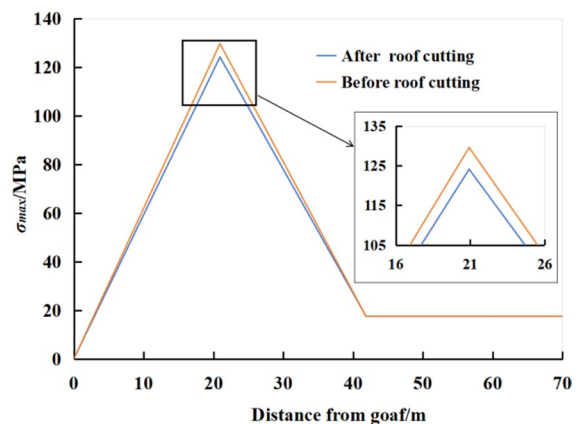


Fig. 8 Side abutment stress distribution curve before and after roof cutting

4.3 Analysis of the Influencing Factors of Roof Cutting and the Stress Relief Effect

Figure 9 shows the change in the peak value of the side abutment stress of the working face before and after roof cutting under the influence of different fracture zone heights when L_t was 60 m and remained unchanged. The figure shows that the side abutment stress of the working face was significantly affected by the development height of the fracture zone, and the larger the height of the fracture zone was, the smaller the peak value of the side abutment stress before and after roof cutting. The main reason was that the greater the development height of the fracture zone was, the greater the load of the broken rock mass in the middle of the goaf supported by the floor, which reduced the additional load of the roof on the side coal body of the goaf. Moreover, as the development height of the fracture zone increased, the degree of reduction in the peak abutment stress on the side after roof cutting also increased. When the development heights of the fracture zone were 60 m, 80 m, 100 m, and 120 m, the reductions in the peak abutment stress were 7.75 MPa, 7.87 MPa, 7.95 MPa, and 8.00 MPa, respectively. The stress reduction shows a power function growth trend with increasing fracture zone height.

Figure 10 shows the variation in the peak side abutment stress before and after roof cutting under the influence of different cantilever lengths (L_t), with the development height H_f of the fracture zone of 115 m. As shown in the figure, before cutting the roof, the

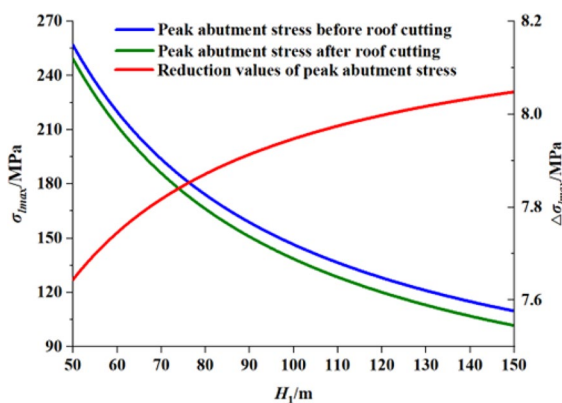


Fig. 9 Peak values of the side abutment stress under different H_f conditions

side abutment stress of the working face continuously increases with increasing cantilever length L_t and shows a linear growth trend. This was mainly because the longer the cantilever length was, the more the roof load was transmitted to the side coal body of the goaf through the hard roof. The cantilever length L_t has no effect on the side abutment stress of the working face after roof cutting. Therefore, the longer the cantilever length is, the greater the decrease in the side abutment stress after roof cutting. When the cantilever length was 30 m, 40 m, and 50 m, the peak reduction values of the side abutment stress after roof cutting were 4.11 MPa, 5.48 MPa, and 6.85 MPa, respectively. The stress reduction shows a linear growth trend with increasing cantilever length.

4.4 Analysis of the Numerical Simulation Results

Figure 11a, b show the stress distribution nephograms of the stope before and after roof cutting, respectively. From the diagram, it can be seen that the stress concentration area appears in the front and side of the goaf during the process of mining the working face, and the vertical stress near the end of the working face on the roof cutting side is less than that of the uncutting roof. Figure 11c, d show the vertical stress distribution curve 5 m in front of the working face and 100 m behind the working face, respectively. The survey line was arranged perpendicular to the advancing direction of the working face. It can be seen from the diagram that the advanced abutment stress and the side abutment stress on the roof cutting side both

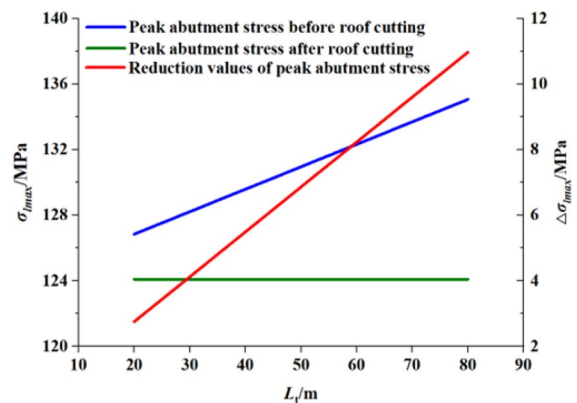


Fig. 10 Peak values of the side abutment stress under different L_t conditions

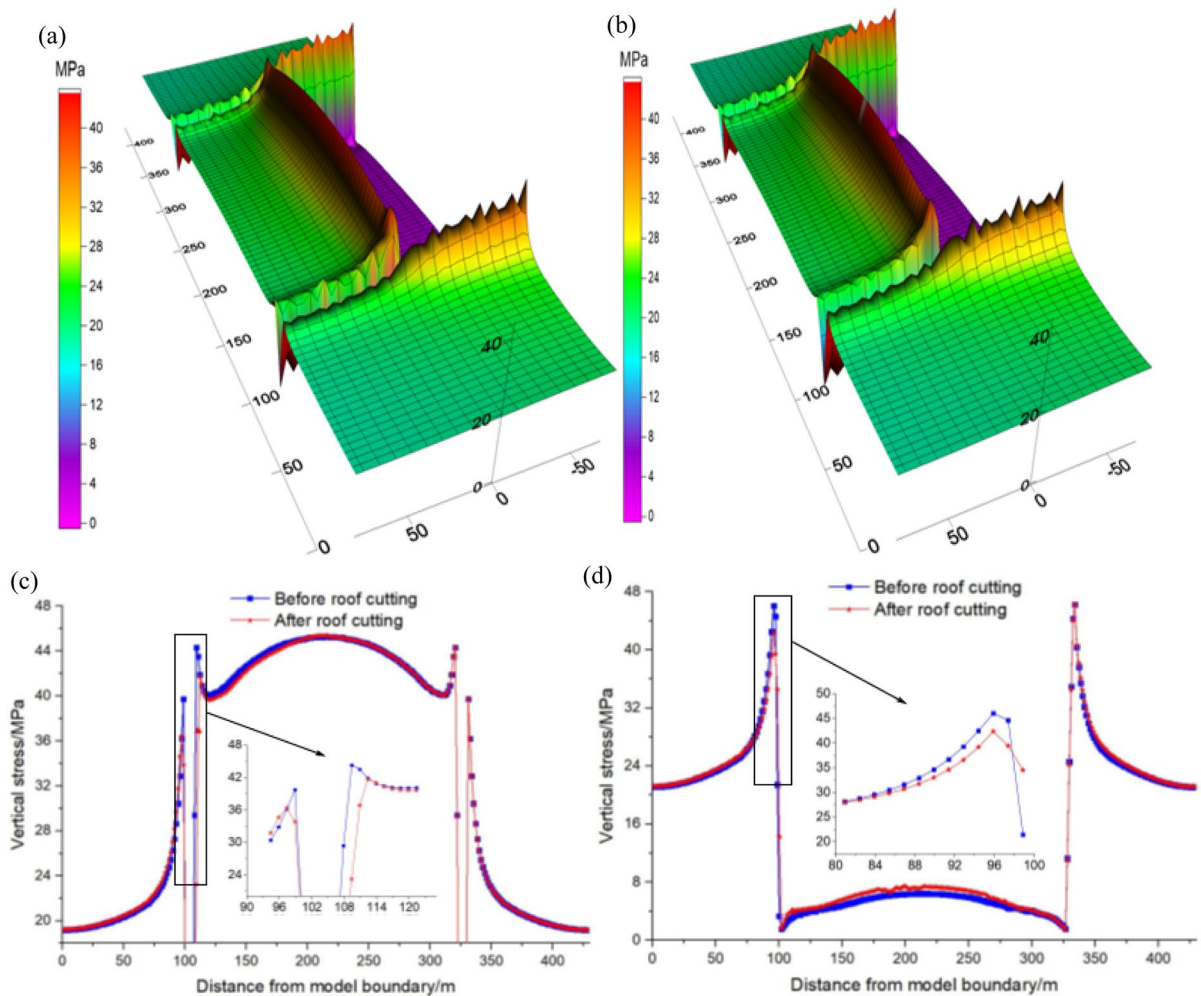


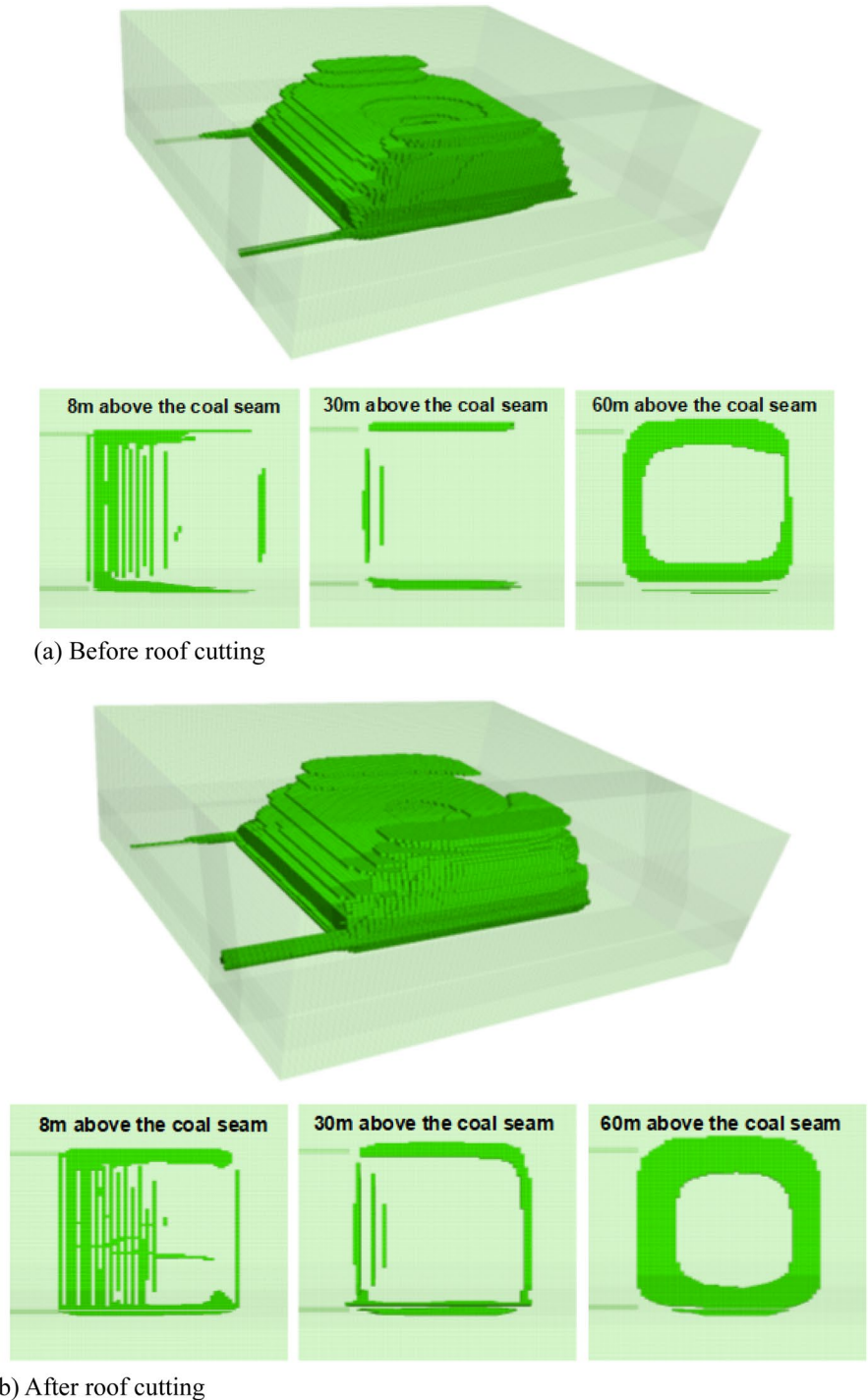
Fig. 11 Stress distribution of the stope. **a** Stress nephograms of the stope before roof cutting, **b** stress nephograms of the stope after roof cutting, **c** vertical stress distribution curve 5 m

decreased after roof cutting. The maximum vertical stresses on both sides of the roadway 5 m in front of the working face were 44.3 MPa and 41.7 MPa. After roof cutting, the maximum vertical stresses on both sides of the roadway decreased to 39.7 MPa and 36.4 MPa. The maximum side vertical stress in the goaf 100 m behind the working face before roof cutting was 44.6 MPa, and the side vertical stress in the goaf 100 m behind the working face after roof cutting was reduced to 42.4 MPa. The numerical simulation results verified that roof cutting can effectively reduce the abutment stress of the mining area, and the research conclusion was consistent with the theoretical analysis results.

in front of the working face, **d** vertical stress distribution curve 100 m behind the working face

Figure 12 shows the nephograms of the plastic differentiation of the stope before and after roof cutting. The figure shows that the development range of the plastic zone of the roof after roof cutting was significantly larger than that before roof cutting. According to the distribution maps of plastic zones at 8 m and 30 m above the coal seam, the plastic zone near the end of the working face was not fully developed before roof cutting, and the roof stratum above the end of the working face could not completely break and was still in a suspended state. However, after roof cutting, the plastic zone above the end of the working face continues to develop, and the roof stratum completely breaks. Therefore, roof cutting was conducive

Fig. 12 The distribution law of the plastic zone in the stope. **a** Before roof cutting, **b** after roof cutting



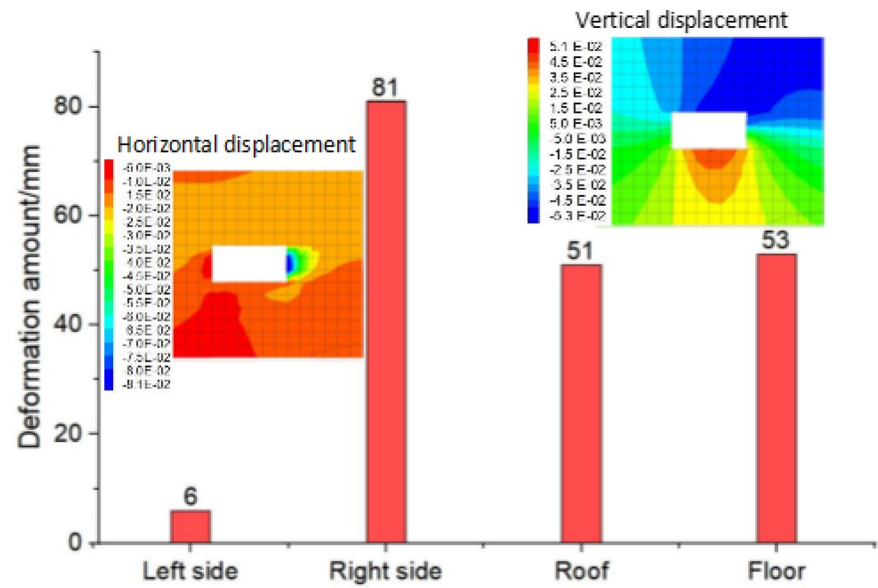
to the development and penetration of the plastic zone of the roof, which can promote the breaking and sinking of the roof and prevent the development of a large area of suspended roof near the end.

Figure 13 shows the deformation of the roadway before and after roof cutting. The figure shows that the deformation of the right side of the roadway before roof cutting (the working face side of the

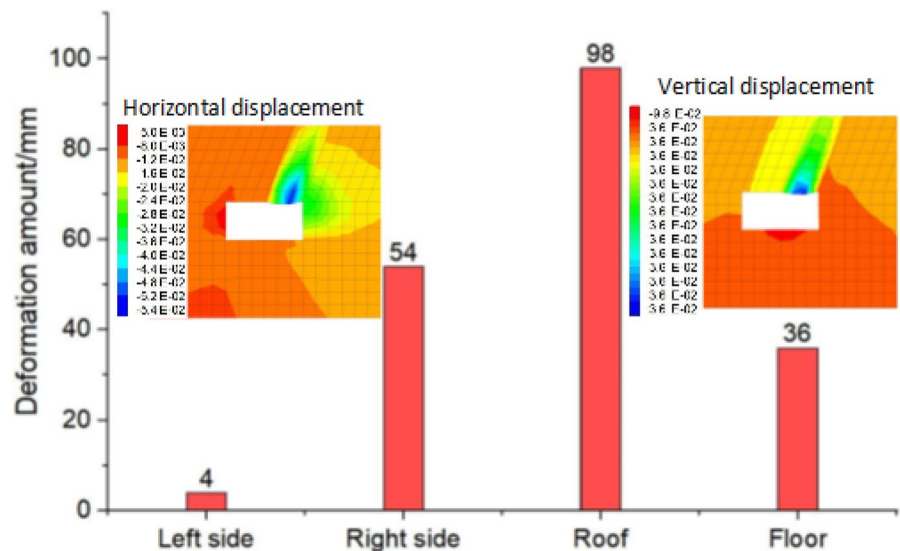
roadway) was the largest, and the horizontal displacement was 81 mm. The second factor is the floor heave of the roadway, which was 53 mm, the roof subsidence of the roadway was 51 mm, and the deformation of the left side of the roadway was the smallest, at only 6 mm. After roof cutting, the roof subsidence of the roadway increased. Although the roof subsidence of the roadway increased from 51 to 98 mm, only near the cutting hole did the roof subsidence increase,

not that of the whole roadway roof. The subsidence of the roadway roof outside the influence area of the borehole does not increase significantly. Therefore, roof cutting will not cause roadway roof instability. After roof cutting, the horizontal displacement of the left side of the roadway was reduced to 5 mm, which is a reduction of 20.0%. The horizontal displacement of the right side of the roadway was reduced to 54 mm, a 33.3% reduction. The floor heave of the

Fig. 13 Roadway deformation before and after roof cutting. **a** Before roof cutting, **b** after roof cutting



(a) Before roof cutting



(b) After roof cutting

roadway was reduced to 36 mm, which is a decrease of 32.1%. In summary, roof cutting can effectively inhibit the deformation of the two sides and the floor of the roadway.

5 Discussion

When evaluating the effect of roof cutting, field measurement methods, such as drilling peeps, borehole stress meter monitoring and drilling cutting method evaluation are often used (Szlązak et al. 2022; Xie et al. 2023; Sobczyk 2014; Ray et al. 2018; Pang et al. 2022). The development of roof cracks after roof blasting cutting can be visually observed in drilling peeps. The peep borehole was located at the midpoint of the connection between the two blasting boreholes.

The drilling results are shown in Fig. 14. It can be seen from the diagram that the roof cracks in the drilling area were relatively developed after blasting roof cutting, indicating that the blasting had a good roof cutting effect. Figure 15 shows the goaf behind the working face. The figure shows that under the influence of blasting roof cutting, the integrity of the roof was reduced, and the hard roof could collapse in time to avoid the formation of a large area of suspended roof. Borehole stress meter monitoring and drilling cutting method tests aim to evaluate the pressure relief effect of the stope after roof cutting, but field monitoring has a high labor intensity and strong data dispersion. In this paper, a theoretical analysis method was used to compare and analyze roof structure models before and after roof cutting, and an expression of the side abutment stress distribution before and after

Fig. 14 Peep borehole view of roof drilling

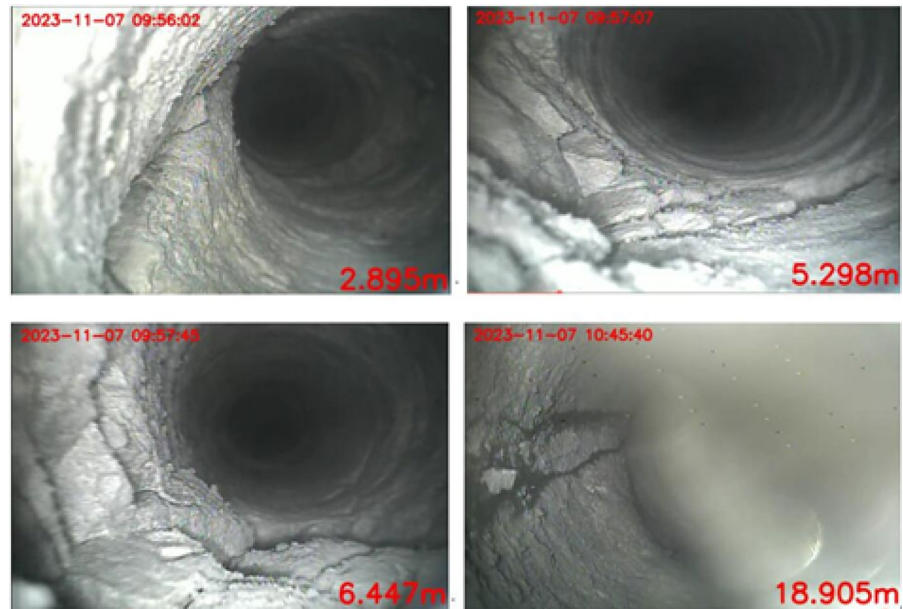


Fig. 15 Roof strata caving in the goaf



roof cutting was established. The reduction degree of the side abutment stress after roof cutting was quantified, and the influence of the fracture zone height and cantilever length of the roof on the pressure relief effect was analyzed, which provides a new approach for evaluating the effect of roof cutting and pressure relief.

Roadways are the main areas for rockbursts or other dynamic disasters, and the main purpose of cutting hard roofs is to maintain roadway stability. The numerical simulation method was used to compare and analyze the evolution of the stress, roof plastic zone and deformation of roadways under the action of roof cutting. The stress of the surrounding rock of a roadway decreases after roof cutting, the deformation of the two sides and the floor of the roadway is significantly reduced, and the stability of the roadway is greatly improved. Therefore, after roof cutting and stress relief at Panel 11,618 (east) of the Xieqiao Coal Mine, the advance support single pillar of the roadway was removed, greatly reducing the labor intensity of workers and the support cost of the roadway. Figure 16a shows the advanced support and deformation of the roadway without roof cutting and pressure relief (Jiang et al. 2016), and Fig. 16b shows the deformation of the roadway after roof cutting pressure relief in the Xieqiao Coal Mine.

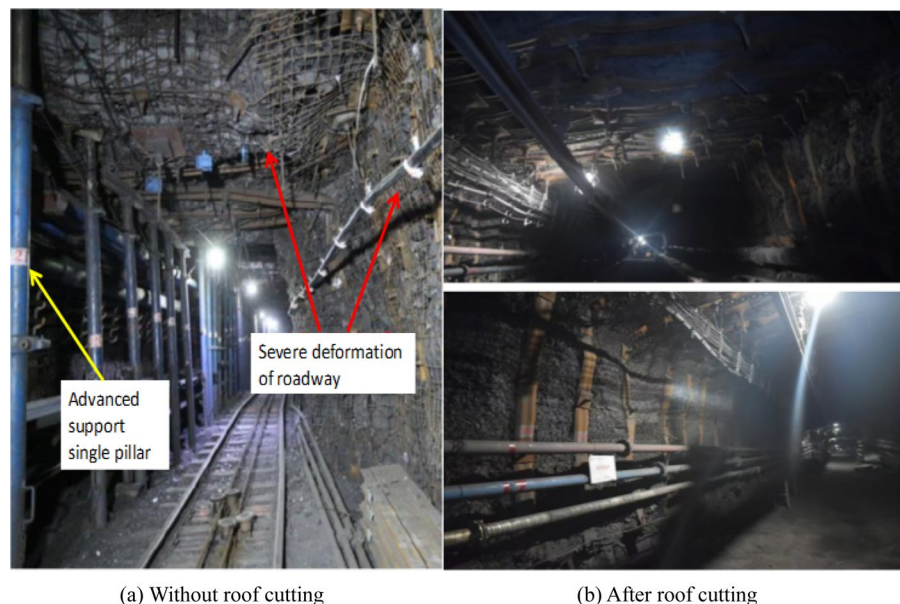
Figure 17 shows the deformation of the roadway monitored on site during mining. When the distance

between the working face and the measuring point was 150–75 m, the deformation of the roadway increased slowly. When the distance between the working face and the measuring point was less than 75 m, the deformation of the roadway increased significantly. The floor heave of the roadway was the largest, and that of the right side of the roadway (the side of the working face) was the second largest, while the deformation of the left side of the roadway was slightly smaller than that of the right side of the roadway, and the roof subsidence of the roadway was the smallest. The field test results are consistent with the numerical simulation results, and the stability of the mining roadway was good during the service period. The advance support of the roadway can be cancelled to ensure the stability of the roadway after roof cutting and pressure relief.

6 Conclusions

Using the 11,618 (east) working face of the Xieqiao Coal Mine as the engineering background, in which the hard roof directly overlies the coal seam, mechanical models of the roof structure were constructed before and after roof cutting. The load transfer behavior of the roof strata was revealed, and an expression for the side abutment stress distribution near the end of the working face before and after roof cutting was

Fig. 16 Diagrams of roadway support and deformation before and after roof cutting. **a** Without roof cutting, **b** After roof cutting



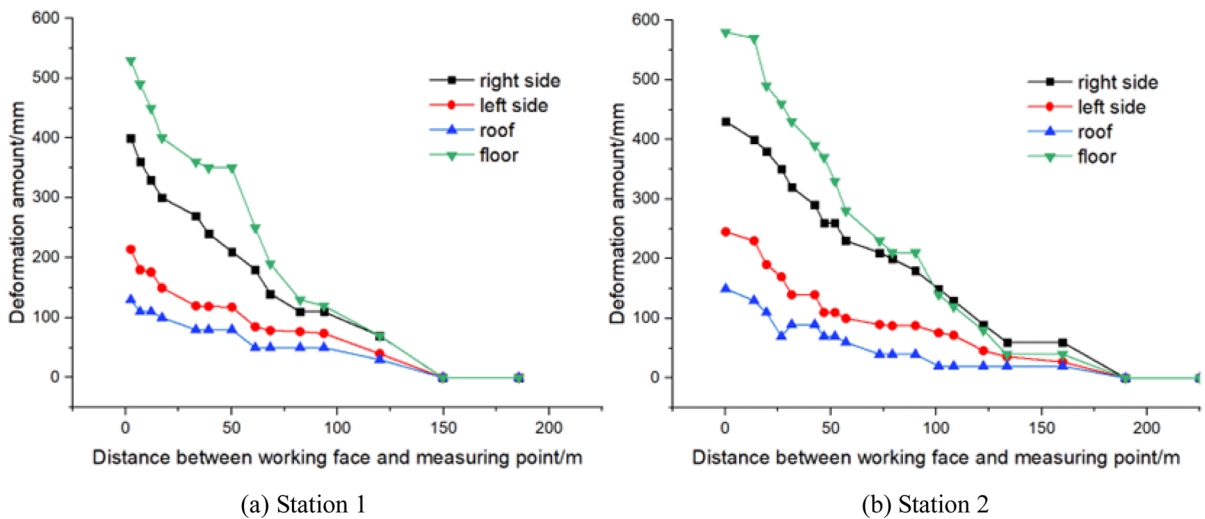


Fig. 17 Roadway deformation field monitoring results. **a** Station 1, **b** station 2

established. The influence of the height of plastic zone development and the cantilever length of the hard roof on the pressure relief effect of roof cutting was analyzed. The stress reduction showed a power function growth trend with increasing crack zone height and a linear growth trend with increasing cantilever length of the hard roof. The results of the theoretical analysis provided a new idea and method for evaluating the effect of roof cutting and stress relief.

The FLAC3D numerical simulation method was used to study the influence of roof cutting on the stope stress, plastic zone and surrounding rock stability of the roadway. After roof cutting, both the advanced abutment stress and the side abutment stress of the working face decreased, and the research results were consistent with the theoretical analysis results. After roof cutting, the range of the plastic zone of the roof increased, and the roof was more likely to break and sink, which prevented a large area of hard roof hanging. After cutting the roof, the deformation of both sides of the roadway and the bulging of the floor both decreased. The subsidence of the roadway roof increased only near the blasting borehole. Therefore, cutting the roof to relieve pressure not only reduces the stress in the mining area but also has a restraining effect on roadway deformation.

Theoretical analysis and numerical results showed that roof cutting can not only reduce the stress of the stope but also reduce the deformation and improve the stability of the roadway. Therefore, after roof cutting

and stress relief at Panel 11,618 (east) of the Xie-qiao Coal Mine, the advance support single pillar of the roadway was removed, greatly reducing the labor intensity of workers and the support cost of the roadway. Through drilling, it was found that cracks developed on the roof after cutting, and the roof behind the working face could collapse in a timely manner. The deformation of the roadway was relatively small, and good stability was maintained during the service period.

Roof cutting and pressure relief are important means to control dynamic disasters and maintain roadway stability in deep mine mining and have great application value. However, there are still some problems that need to be further studied. For example, the operation process of blasting roof cutting is complex, and the labor intensity of drilling, charging, and sealing operations is high. In addition, roof cutting not only reduces the static load stress level of the stope but also reduces the dynamic load released by hard roof breaking. Therefore, the influence of roof cutting on the dynamic load of roof breaking requires further study.

Author Contributions All authors contributed to the study conception and design. Material preparation, data collection and analysis were performed by KP, LC and JR. The first draft of the manuscript was written by KP and LC, and the manuscript was reviewed by YD and LS. All authors commented on previous versions of the manuscript. All authors read and approved the final manuscript.

Funding The research of this study was sponsored by the National Natural Science Foundation of China Youth Project (52304074), the Natural Science Foundation of Anhui Province (2208085QE144), the National Natural Science Foundation of China (U21A20110), the Open Fund of Engineering Laboratory for Safe and Precise Coal Mining of Anhui Province (ESCMP202308). Start-up Fund for Introducing Talents and Scientific Research of Anhui University of Science and Technology.

Data availability The data used to support the findings of the study are available from the corresponding author upon request.

Declarations

Conflict of interest The authors confirm there is no conflict of interest in the manuscript.

Ethical approval This article does not contain any studies with human participants or animals performed by any of the authors.

References

- Ahmet GY, Murat K (2022) A new protective destressing technique in underground hard coal mining. *Int J Rock Mech Min Sci* 130:104327. <https://doi.org/10.1016/j.ijrmms.2020.104327>
- Dang JX, Tu M, Zhang XY, Bu QW (2024) Research on the bearing characteristics of brackets in thick hard roof mining sites and the effect of blasting on roof control. *Geomech Geophys GeoEnergy GeoResources* 10(1):18. <https://doi.org/10.1007/s40948-024-00735-3>
- Ganesan G, Mishra AK (2024) A modified anisotropic hoek and brown failure criterion for transversely isotropic rocks. *Geotech Geol Eng.* <https://doi.org/10.1007/s10706-024-02818-0>
- Ghosh GK, Sivakumar C (2018) Application of underground microseismic monitoring for ground failure and secure longwall coal mining operation: a case study in an Indian mine. *J Appl Geophys* 150:21–39. <https://doi.org/10.1016/j.jappgeo.2018.01.004>
- Guo PF, Deng SW, Jin ZP, Zhu XY, Wang YY, Ta B, Kong XW (2024) Mine pressure behavior of gob-side entry retaining by roof cutting in closely spaced coal seams. *Geotech Geol Eng* 42:611–630. <https://doi.org/10.1007/s10706-023-02592-5>
- Jiang LS, Sainoki A, Mitr HS, Ma NJ, Liu HT, Zhen H (2016) Influence of fracture-induced weakening on coal mine gateroad stability. *Int J Rock Mech Min Sci* 88:307–317. <https://doi.org/10.1016/j.ijrmms.2016.04.017>
- Karolina AK, Pawel D (2021) Influence of driving direction on the stability of a group of headings located in a field of high horizontal stresses in the polish underground copper mines. *Energies* 14(18):5955. <https://doi.org/10.3390/en14185955>
- Ko Y, Shin C, Jeong Y, Cho S (2022) Blast hole pressure measurement and a full-scale blasting experiment in hard rock quarry mine using shock-reactive stemming materials. *Appl Sci* 12(17):8629. <https://doi.org/10.3390/app12178629>
- KonicekSoucekStasSingh PKLR (2013) Long-hole destress blasting for rockburst control during deep underground coal mining. *Int J Rock Mech Min Sci* 61:141–153. <https://doi.org/10.1016/j.ijrmms.2013.02.001>
- Kumar R, Mishra AK, Kumar A, Singh AK, Ram S, Singh AK, Singh R (2022) Importance of fracturing hard and massive overlying strata for complete extraction of thick coal seam—case studies. *J Geol Soc India* 98(2):203–210. <https://doi.org/10.1007/s12594-022-1960-y>
- Kumar S, Sinha RK, Jawed M, Murmu S (2024) Assessment of coal pillar strength under the influence of sand stowing in deep coal mines. *Geotech Geol Eng* 42:2815–2831. <https://doi.org/10.1007/s10706-023-02707-y>
- Mishra Arvind K, Mishra Awadh K, Rout M (2013) Blast-induced caving from surface over continuous miner panel at a 110 m cover in an indian mine. *Arab J Sci Eng* 38:1861–1870. <https://doi.org/10.1007/s13369-012-0386-z>
- Mondal D, Roy PNS, Behera PK (2017) Use of correlation fractal dimension signatures for understanding the overlying strata dynamics in longwall coal mines. *Int J Rock Mech Min Sci* 91:210–221. <https://doi.org/10.1016/j.ijrmms.2016.11.019>
- Osipov AA (2017) Fluid mechanics of hydraulic fracturing: a review. *J Pet Sci Eng* 156:513–535. <https://doi.org/10.1016/j.petrol.2017.05.019>
- Pang BX, Liu ZB, Liu X, Wang X, Wang F, Li KM, Lu HL (2022) Effect of crooked drill pipe rotation on cuttings transport in horizontal directional drilling using kinetic theory of granular flow—a numerical perspective. *Tunn Undergr Space Technol* 128:104665. <https://doi.org/10.1016/j.tust.2022.104665>
- Rajwa S, Janoszek T, Prusek S (2019) Influence of canopy ratio of powered roof support on longwall working stability—a case study. *Int J Min Sci Technol* 29(4):591–598. <https://doi.org/10.1016/j.ijmst.2019.06.002>
- Ray P, Srinivasan B, Balasubramaniam K, Rajagopal P (2018) Monitoring pipe wall integrity using fiber Bragg grating-based sensing of low-frequency guided ultrasonic waves. *Ultrasonics* 90:120–124. <https://doi.org/10.1016/j.ultras.2018.06.009>
- Sainoki A, Emad MZ, Mitri HS (2017) Study on the efficiency of destress blasting in deep mine drift development. *Can Geotech J* 45(4):518–528. <https://doi.org/10.1139/cgj-2016-0260>
- Shang XG, Zhu ST, Jiang FX, Liu JH, Li JJ, Hitch M, Liu HL, Tang SB, Zhu C (2022) Study on dynamic disaster mechanisms of thick hard roof induced by hydraulic fracturing in surface vertical well. *Minerals* 12(12):1537. <https://doi.org/10.3390/min12121537>
- Sobczyk J (2014) A comparison of the influence of adsorbed gases on gas stresses leading to coal and gas outburst. *Fuel* 115:288–294. <https://doi.org/10.1016/j.fuel.2013.07.016>
- Sun B, Zhu ST, Jiang FX, Wang GA (2022) Mechanism and safety mining technology of overall instability-induced rockbursts of multi-coal seam spatially isolated working

- face. *Math Probl Eng*. <https://doi.org/10.1155/2022/1038139>
- Sun XM, Qi ZM, Zhang Y, Li ZH, Xie C, Yang JK, Ding JX, He LS (2024) Characteristics and control measures of deep and shallow dense drilling in roadway for pressure relieving by cutting roof. *Min Metall Explor* 41:787–803. <https://doi.org/10.1007/s42461-024-00940-4>
- Szlazak N, Korzec M, Piergies K (2022) The determination of the methane content of coal seams based on drill cutting and core samples from coal mine roadway. *Energies* 15(1):178. <https://doi.org/10.3390/en15010178>
- Vennes I, Mitri H, Chinnasane DR, Yao M (2020) Large-scale distress blasting for seismicity control in hard rock mines: a case study. *Int J Min Sci Technol* 30(2):141–149. <https://doi.org/10.1016/j.ijmst.2020.01.005>
- Wang Q, Qin Q, Jiang B, Jiang ZH, He MC, Li SC, Wang Y (2020) Geomechanics model test research on automatically formed roadway by roof cutting and pressure releasing. *Int J Rock Mech Min Sci* 135(1):104506. <https://doi.org/10.1016/j.ijrmms.2020.104506>
- Wang Q, Jiang ZH, Jiang B, He MC, Yang J, Xue HJ (2023) Ground control method of using roof cutting pressure release and energy-absorbing reinforcement for roadway with extra-thick hard roof. *Rock Mech Rock Eng* 56:7197–7215. <https://doi.org/10.1007/s00603-023-03461-6>
- Wojtecki L, Golda I (2020) A comparison of the seismic effects of different blasting types executed during the longwall mining of a coal seam. *J Min Sci* 56:947–961. <https://doi.org/10.1134/S1062739120060071>
- Wojtecki L, Konicek P, Mendecki MJ, Golda I, Zuberek WM (2020) Geophysical evaluation of effectiveness of blasting for roof caving during longwall mining of coal seam. *Pure Appl Geophys* 177(2):905–917. <https://doi.org/10.1007/s00024-019-02321-1>
- Xie ZZ, Zhang N, Qian DY, Han CL, An YP, Wang Y (2018) Rapid excavation and stability control of deep roadways for an underground coal mine with high production in inner mongolia. *Sustainability* 10:1160. <https://doi.org/10.3390/su10041160>
- Xie XP, Fang XQ, Liu HY, Xing XP, Liang MF, Wu G, Chen NN (2023) Development and application of a borehole stress meter in rocks surrounding the roadway, based on optical-fiber sensing technology. *Front Earth Sci* 10:1122579. <https://doi.org/10.3389/feart.2022.1122579>
- Xu JZ, Zhai C, Ranjith PG, Sun Y, Qin L, Ma HT, Guo JS, Ma Z (2019) Investigation of non-explosive expansion material in roof caving field application. *Int J Rock Mech Min Sci* 120:50–57. <https://doi.org/10.1016/j.ijrmms.2019.05.004>
- Xu XH, He FL, Zhai WL, Wang DQ, Lin XB, Song JY, Zhang YJ (2023) Pressure bearing and deformation of the surrounding rock-support body and control technology on the gangue side in gob side entry retaining by roof cutting. *Chin J Rock Mech Eng*. <https://doi.org/10.13722/j.cnki.jrme.2023.0386>
- Zabolotnii E, Morgenstern NR, Wilson GW (2021) Mesh sensitivity in numerical models of strain-weakening systems. *Comput Geotech* 136:104253. <https://doi.org/10.1016/j.compgeo.2021.104253>
- Zhang LX, Yi L, Gang L, Liu GC, Deng ZH, Mi JL (2024) Evolutionary law and regulatory technology of roof migration on gob-side entry retaining. *Sci Rep* 14(1):5581. <https://doi.org/10.1038/s41598-024-56108-z>
- Zhao TB, Zhang PF, Zhang XF, Guo WY, Gong XF, Gu XB, Guo CQ (2024) Microseismic behavior during mining of the working face under blasting presplitting of a hard roof. *Int J Geomech* 24(3):05024001. <https://doi.org/10.1061/ijgnai.gmeng-9042>

Publisher's Note Springer Nature remains neutral with regard to jurisdictional claims in published maps and institutional affiliations.

Springer Nature or its licensor (e.g. a society or other partner) holds exclusive rights to this article under a publishing agreement with the author(s) or other rightsholder(s); author self-archiving of the accepted manuscript version of this article is solely governed by the terms of such publishing agreement and applicable law.